International Journal of Rotating Machinery 2005:1, 23–29


# CFD Analysis of the First-Stage Rotor and Stator in a Two-Stage Mixed Flow Pump

**Steven M. Miner**
*Mechanical Engineering Department, United States Naval Academy, Annapolis, MD 21402, USA*
*Email: miner@usna.edu*

*Received 30 March 2004*

A commercial computational fluid dynamics (CFD) code is used to compute the flow field within the first-stage rotor and stator of a two-stage mixed flow pump. The code solves the 3D Reynolds-averaged Navier-Stokes equations in rotating and stationary cylindrical coordinate systems for the rotor and stator, respectively. Turbulence effects are modeled using a standard $k - \varepsilon$ turbulence model. Stage design parameters are rotational speed 890 rpm, flow coefficient $\phi = 0.116$, head coefficient $\psi = 0.094$, and specific speed 2.01 (5475 US). Results from the study include velocities, and static and total pressures for both the rotor and stator. Comparison is made to measured data for the rotor. The comparisons in the paper are for circumferentially averaged results and include axial and tangential velocities, static pressure, and total pressure profiles. Results of this study show that the computational results closely match the shapes and magnitudes of the measured profiles, indicating that CFD can be used to accurately predict performance.

**Keywords and phrases:** mixed flow pump, CFD, viscous, rotor, stator.

## 1. INTRODUCTION

Designers are continually being challenged to provide pumps that operate more efficiently, quietly, and reliably at lower cost. Key to building these machines is a better understanding of, and ability to, predict their hydraulic and dynamic characteristics. Understanding and predicting these characteristics requires a detailed knowledge of the flow fields within the stationary and rotating passages of the pump. With the advent of more powerful computers, computational fluid dynamics (CFD) is seeing more and more use in predicting the flow fields in both the stationary and rotating passages of turbomachines. Lakshminarayana [1] provides a review of the techniques that are currently being used as well as an assessment of the state of the art.

Most of the previous work in this area has been for compressible flow and was driven by the gas turbine industry. Adamczyk et al. [2] and Furukawa et al. [3] are typical examples. Examples of incompressible studies are [4] and [5]. In both cases, compressible and incompressible flow, the solutions have been obtained using codes that are developed in house, using meshes that have in excess of 100 000 nodes, and are run on super computer platforms. The hardware and time requirements for models of this size are not suitable for use in day-to-day design applications.

The present work uses FLOTRAN to obtain solutions for the flow field and pressure field within the impeller and stator of a mixed flow pump. The code is run on a Sun SparcStation 20, and the model size is approximately 26 000 nodes for the impeller and 21 000 nodes for the stator. Turn around time for geometry update and solution is one day for each component, which makes the use of the code in the design process feasible. Results presented here include circumferentially averaged velocity and pressure profiles at the leading and trailing edges of the impeller and stator. This study is a continuation of work performed by White et al. [6] and Miner [7], which considered an axial flow impeller. In addition, Miner [8] considered the impeller by itself for this mixed flow geometry. The mixed flow geometry is being evaluated because of its increase in head coefficient.

## 2. CFD FORMULATION

FLOTRAN is a finite-element-based code which solves the Reynolds-averaged Navier-Stokes equations in a primitive variable form. Turbulence is modeled using the $k - \varepsilon$ turbulence model, with the log law of the wall to simulate the boundary layers. The formulation of the code is based on the SIMPLER method of Patankar [9]. For the impeller analysis discussed in this paper the equations governing the turbulent

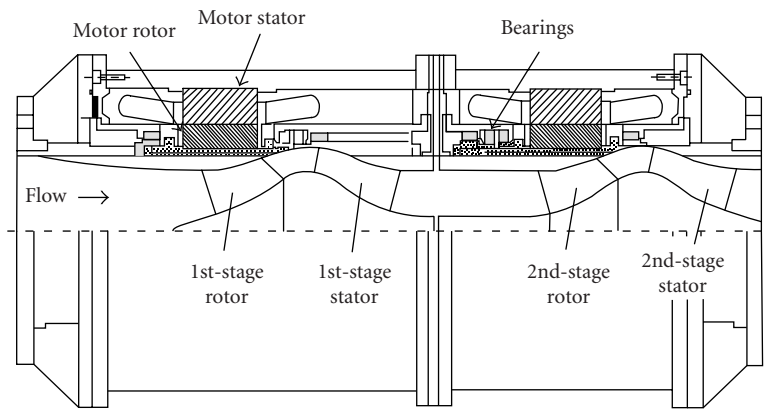


Figure 1: Pump cross-section.

incompressible flow are formulated in a rotating reference frame. The continuity and momentum equations become

$$\nabla \bullet (\rho \vec{U}) + \frac{\partial \rho}{\partial t} = 0,$$
$$\frac{D(\rho \vec{U})}{Dt} + 2\rho \vec{\omega} \times \vec{U} + \rho \vec{\omega} \times \vec{\omega} \times \vec{r} = \rho \vec{g} - \nabla P + \mu_e \nabla^2 \vec{U}, \tag{1}$$

where $P$ is modified to account for effects due to rotation, and $\mu_e$ is the linear combination of the kinematic viscosity and the turbulent viscosity derived from the $k-\varepsilon$ model. For the stator the equations are formulated in the stationary reference frame. The form of the continuity equation remains the same but the momentum equation reduces to

$$\frac{D(\rho \vec{U})}{Dt} = \rho \vec{g} - \nabla P + \mu_e \nabla^2 \vec{U}. \tag{2}$$

These equations along with the appropriate boundary conditions are solved for the three components of velocity and the pressure. Boundary conditions used for this analysis include stationary and moving walls, specified inlet velocities, specified outlet pressure, and periodic boundaries.

## 3. GEOMETRY

Figure 1 shows a cross-section view of the pump, which is described in detail by White et al. [6], the only difference being that the axial flow impellers have been replaced by mixed flow impellers. The pump is a two-stage design with an impeller and stator making up each stage. The impellers are contrarotating. The analysis presented in this paper is for the first-stage impeller and stator. Design parameters for the stage are rotational speed 890 rpm, flow rate 0.38 $m^3/s$, and head rise 13.1 m. These result in the following nondimensional parameters: flow coefficient $\phi = 0.116$, head coefficient $\psi = 0.094$, and specific speed 2.01 (5475 US).

This particular impeller has the shroud attached to the blade tips, which eliminates the blade tip leakage flow. The hub radius varies from 0.037 m at the leading edge to 0.107 m at the trailing edge. The shroud radius varies from 0.126 m at the leading edge to 0.149 m at the trailing edge. Reynold's number based on the blade tip speed at the trailing edge is $1.7 \times 10^6$. For the stator, the hub radius varies from 0.121 m at the leading edge to 0.043 m at the trailing edge. The shroud radii are 0.17 m and 0.126 m for the leading and trailing edges, respectively.

Due to symmetry, only one of the blade passages in the impeller and stator needs to be analyzed. Figure 2 illustrates a generic blade passage with the appropriate upstream and downstream extensions. This becomes the geometry that is modeled in the rotating reference frame for the impeller and in the stationary frame for the stator.

At the inlet to the impeller solution domain, the axial velocity is a constant based on the through flow for the pump. The absolute tangential velocity at the inlet is zero, which implies in the rotating frame that the relative velocity is $-r\omega$, and the radial velocity is zero. The inlet to the solution domain is located approximately twelve chord lengths upstream of the blade leading edge. The only specification made at the outlet is that the static pressure in the absolute frame is uniform and set to zero. This absolute condition is converted into the appropriate relative pressure in the rotating frame. This condition is applied roughly sixteen chord lengths downstream of the blade trailing edge. Periodic boundaries are used upstream and downstream of the blade leading and trailing edges, respectively. For the rotating solid surfaces, all of the velocity components are set to zero. This includes all the surfaces within the blade passage, the nose cone portion of the hub upstream of the blade leading edge, and a short section of the hub, 40% of chord length, downstream of the trailing edge. The shroud surfaces upstream and downstream of the blade passage, and the remaining hub surface downstream are stationary in the absolute reference frame. In the rotating frame they are treated as moving boundaries with the axial and radial components of velocity set to zero and the tangential component set equal to $-r_o\omega$ for the shroud, and $-r_i\omega$ for the hub.

The inlet to the stator solution domain is taken to be 0.013 m upstream of the stator blade leading edge, which is 0.051 m downstream of the impeller blade trailing edge. At this location the axial, radial, and tangential velocity

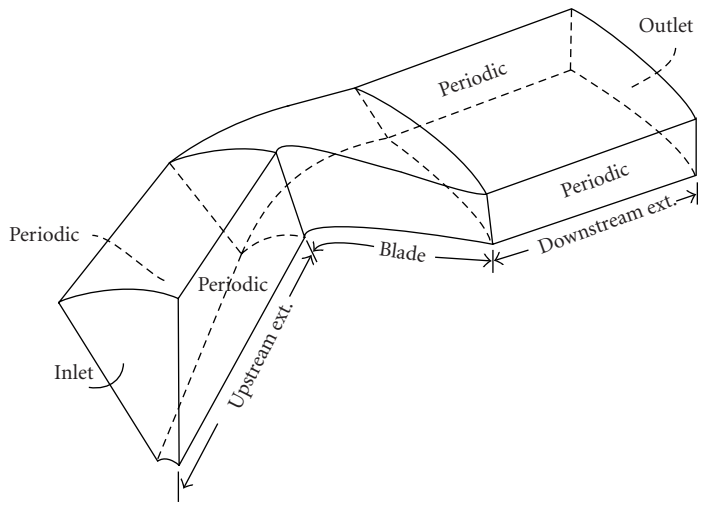


Figure 2: Solution domain.

profiles are input. These velocity profiles are obtained by circumferentially averaging the results for the impeller analysis at this location in the impeller solution domain. No attempt was made to iterate back and forth between the solutions for the impeller and stator. At the outlet, which is roughly sixteen chord lengths downstream of the blade trailing edge, the static pressure is set to zero. At the hub, shroud, pressure, and suction surfaces, the no-slip condition is used. Periodic boundaries are used for the upstream and downstream extensions of the pressure and suction surfaces.

The selection of an appropriate mesh density for this study is based on the previous analysis of an axial flow impeller by Miner [7]. In that study two meshes were considered, one with 22 176 nodes and the other with 40 131 nodes. Comparison of the velocity profiles from the two meshes showed no significant differences. Therefore, it was determined that the coarse mesh provided sufficient resolution. In addition, the computational results for the coarse mesh were compared to measured data for the axial flow impeller. The largest difference between the measured and computed data was 15% in the tangential velocity profile. This difference was due primarily to a difference in the downstream boundary condition used in the model and the conditions downstream of the measured impeller. The computational model considered only the first-stage impeller, whereas the measured data was collected with both of the impellers in place. The experience gained in the analysis of the axial flow impeller was used as the basis for establishing the mesh density in the present analysis. The impeller model has 26 299 nodes with 17 nodes blade to blade, 17 nodes hub to shroud, and 91 nodes inlet to outlet. The stator model has a total of 20 519 nodes with 17 nodes blade to blade, 17 nodes hub to shroud, and 71 nodes inlet to outlet. Both models have the nodes spaced more closely near the hub, shroud, and blade surfaces, as well as near the leading and trailing edges. The value for $y^+$ is between 400 and 600 throughout the blade passage for both models. This value indicates that the near-wall nodes are not within the laminar sublayer but are within the overlap layer of the turbulent boundary layer. Therefore, the application of the log law of the wall formulation is appropriate.

The time required to generate the completed FEA model was approximately 8 hours, the solution for the initial geometry required 500 iterations and 85 hours of CPU time. Subsequent updates to the geometry and an updated solution could be obtained within a day, 8 hours to modify the model and 15 hours to update the solution. Updated solutions were always started from the previous converged solution. Having a one-day turn around time allows CFD analysis to be used in the design process.

## 4. RESULTS

Results for the mixed flow impeller show comparisons between computed and measured profiles 0.35 chord lengths downstream of the impeller trailing edge. Axial and tangential velocity profiles are presented, as well as static and total pressure profiles. The circumferentially averaged velocity results at this location are the inlet conditions for the stator. In the case of the stator, velocity and pressure profiles are presented for a location one chord length downstream of the trailing edge. No measured data was available for the stator. For both the impeller and the stator the data presented are circumferentially averaged. Velocity results are absolute and nondimensionalized by the impeller trailing edge blade tip velocity $U_t$, pressures are nondimensionalized by $\rho U_t^2/2$, and the radius is nondimensionalized by the shroud radius at the trailing edge of the impeller $r_o$.

Figure 3 gives the results of the downstream comparisons for the mixed flow impeller. Comparisons are made to downstream data for both the first- and second-stage impellers. There is no significant difference between the measured results for the two impellers. This indicates that the first-stage stator provides an inflow to the second-stage impeller that matches the inflow condition for the first-stage impeller.

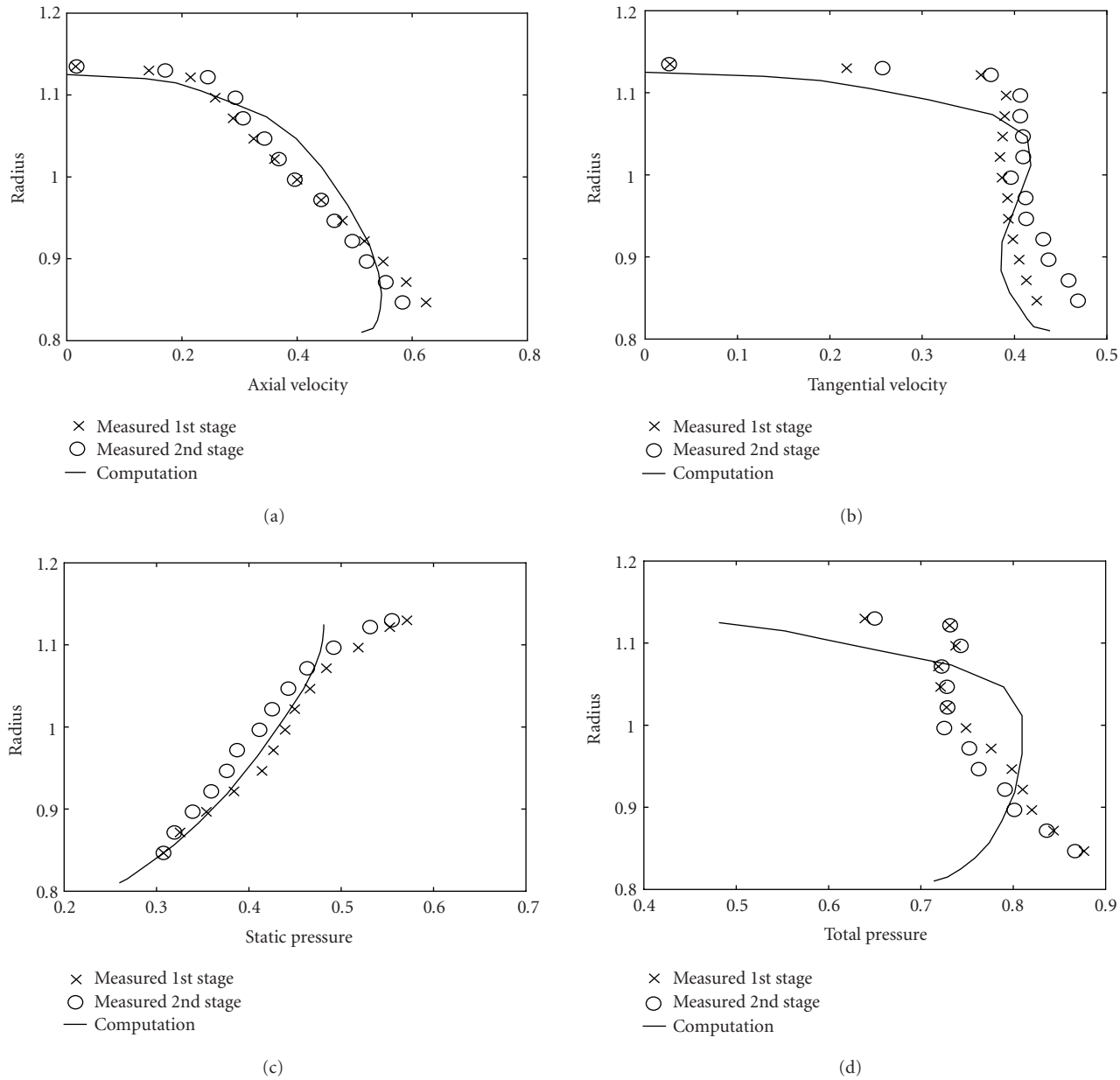


Figure 3: Nondimensional impeller results, downstream location.

Comparing the computed and measured results shows the axial velocities agree to within 12.5% from the hub to the shroud, with the largest difference occurring at the hub. The predicted results show a thicker boundary layer at the hub than the measured results. The measured results for the tangential velocity show more uniform turning of the flow than the predicted results. The largest differences occur at the shroud and are roughly 20%. The primary cause of the difference is the downstream boundary condition in the computation. In the model the shroud is a surface that moves in the opposite direction of the impeller in the rotating frame, and it is extended downstream at a constant radius corresponding to the impeller radius. This moving surface extends to the exit of the solution domain and would tend to increase the relative tangential velocity. Also, the computational model does not include the passage curvature downstream of the impeller. Both these items have an effect on the solution near the shroud surface. Away from the shroud surface the tangential velocities agree to within 8%. The maximum error in the static pressure profile is 16% and occurs at the shroud surface. Away form the shroud the error is less than 3%. The error at the shroud is primarily due to the moving surface boundary condition. The moving boundary causes the relative tangential velocity to be higher than expected, this higher velocity gives rise to a lower static pressure in this region. The agreement between the computed and measured total

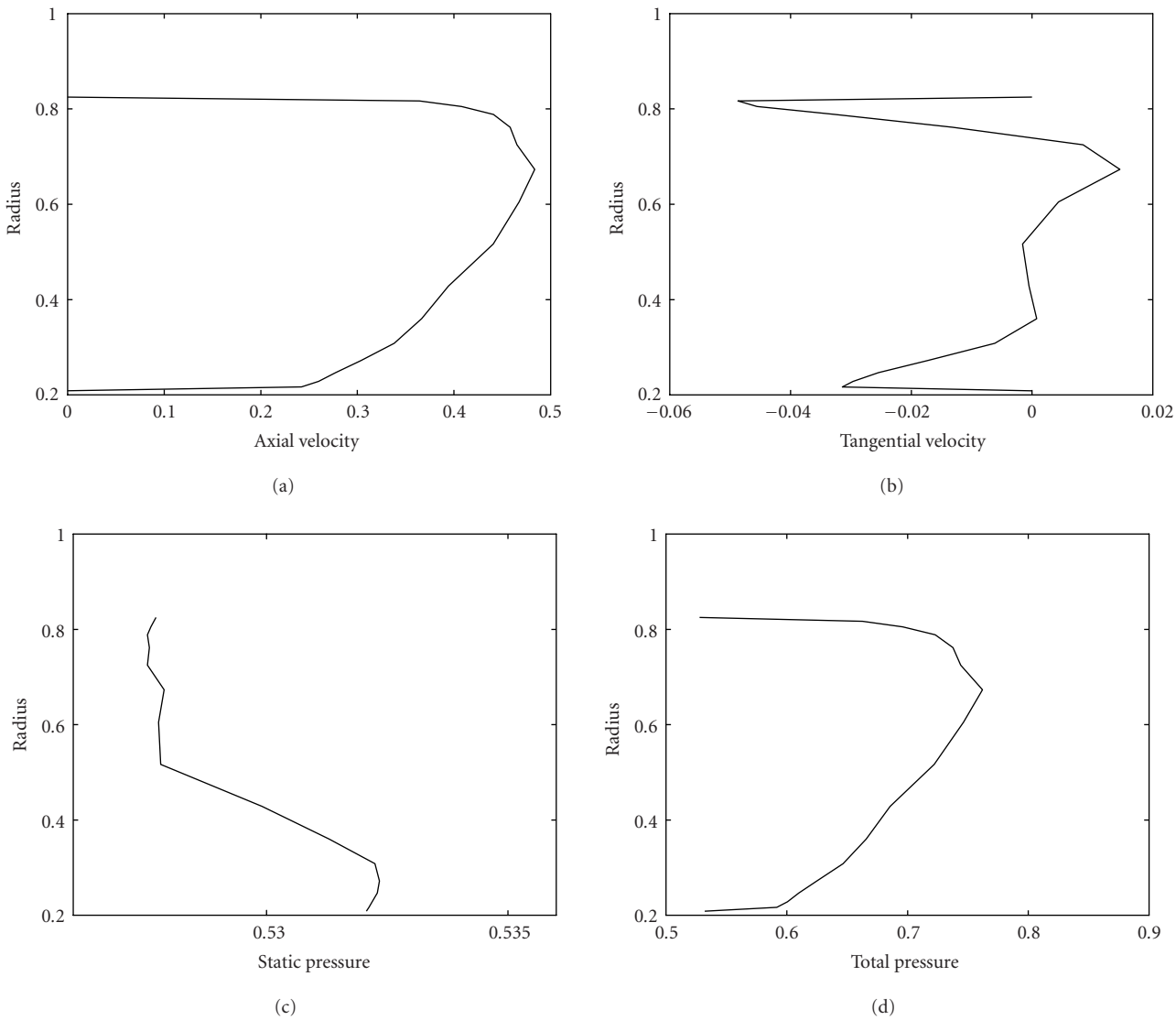


Figure 4: Nondimensional stator results, downstream location.

pressure profiles is not good. The differences at the shroud surface are caused by the disagreement in the tangential velocity at the shroud surface. At the hub surface the differences are due to the disagreement in the axial velocity at the hub surface. However, the difference in the average total pressure is less than 10%.

The stator results are shown in Figures 4 and 5. Figure 4 shows results at the downstream location. The purpose of the first-stage stator is to set up the flow for the second-stage impeller. The desired condition for the impeller inlet is a uniform flow and energy distribution. Comparing the axial velocity profiles downstream of the impeller and stator shows that the stator has reduced the peak velocity and flattened the profile. The stator has removed 95% of the tangential component of velocity from the flow and the static pressure is uniform to within 1% of the mean value. However, the total pressure is only uniform to within 12% of the mean. This is due to the deficit in the axial velocity profile at the hub surface.

Figure 5 shows the comparison between the computational results at the exit of the first-stage stator and the leading edge of the first-stage impeller. This comparison is made because of the comparison between the measured results for the two impellers shown in Figure 3. Both impellers showed similar performance indicating that the inlet conditions to both impellers must be similar. Figure 5 shows that the discharge from the first-stage stator is very similar to the inflow to the first-stage impeller. This would produce performance in the second-stage impeller that would closely match that from the first-stage impeller. The most significant differences occur between the tangential velocity and the static pressure profiles. The tangential velocity profile shows significant preswirl at the impeller leading edge which is due to the rotation of the shroud with the impeller. This preswirl also

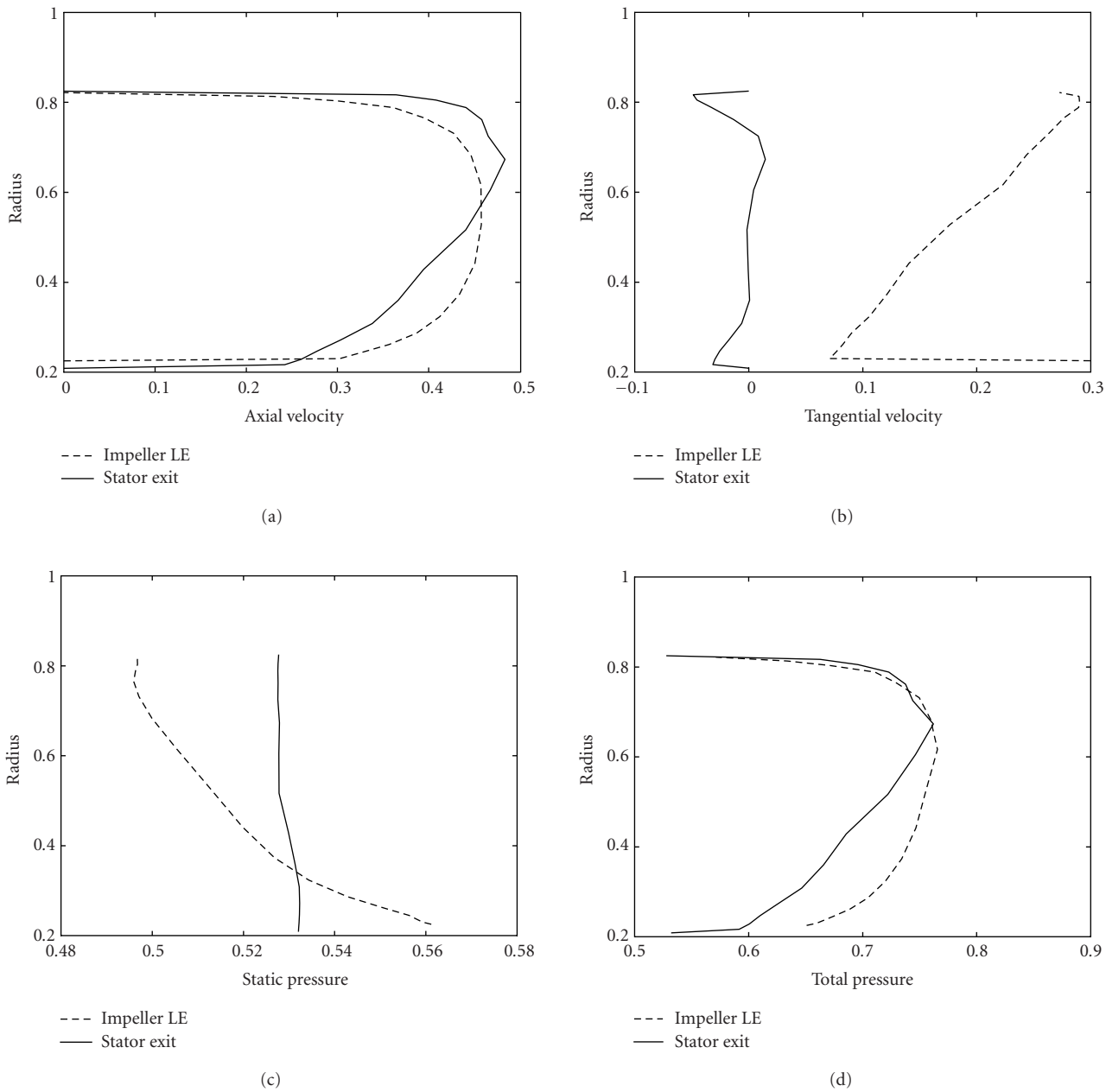


Figure 5: Comparison of stator and impeller results.

influences the shape of the static pressure profile, decreasing from hub to shroud. However, it should be noted that the static pressure profile is still uniform to within 5% of the mean. The differences seen between the total pressure profiles are due primarily to the differences in the axial velocity profiles. The impeller leading edge profile is more uniform from hub to shroud. Some of the bias present in the stator discharge profile would be eliminated in the straight section between the first-stage stator and the second-stage impeller. Overall the computational results for the first-stage indicate that the desired flow is being provided to the second-stage. Again, this is also shown in Figure 3 with the comparison between the measured results for both impellers.

## 5. CONCLUSIONS

The following conclusions are based on the results of this study.

(1) Results from the CFD code showed good agreement with measured results for the mixed flow impeller. The shapes and magnitudes of the velocity and static pressure profiles were correctly predicted.

(2) The largest errors were found in the predictions of the total pressure and were due primarily to the differences in the tangential velocity profiles.

(3) Using circumferentially averaged results from the impeller discharge as the inlet condition for the stator were adequate for performing the stage analysis.

(4) Using small models, CFD can be used effectively in the design process. Turn around times of one day are possible using a work station.

## ACKNOWLEDGMENT

This work was supported by the Naval Surface Warfare Center, Carderock Division, Annapolis Detachment, and the Naval Academy Research Council.

## REFERENCES

[1] B. Lakshminarayana, "An assessment of computational fluid dynamic techniques in the analysis and design of turbomachinery—the 1990 Freeman scholar lecture," *Journal of Fluids Engineering*, vol. 113, no. 3, pp. 315–352, 1991.

[2] J. J. Adamczyk, M. L. Celestina, T. A. Beach, and M. Barnett, "Simulation of 3-D viscous flow within a multi-stage turbine," ASME Paper 89-GT-152, 1989.

[3] M. Furukawa, M. Yamasaki, and M. Inoue, "A zonal approach for Navier-Stokes computations of compressible cascade flow fields using a TVD finite volume method," *ASME Journal of Turbomachinery*, vol. 113, no. 4, pp. 573–582, 1991.

[4] W. S. Yu, B. Lakshminarayana, and D. E. Thompson, "Computation of three-dimensional viscous flow in high Reynolds number pump guide vane," *Numerical Simulations in Turbomachinery*, vol. 227, pp. 117–122, 1995.

[5] C. I. Yang, "A simulation of viscous incompressible flow through a multiple-blade-row turbomachinery with a high-resolution upwind finite differencing scheme," *Numerical Simulations in Turbomachinery*, vol. 227, pp. 11–18, 1995.

[6] J. W. White, J. G. Purnell, and J. G. Stricker, "In-line submersible pump," in *Proc. 2nd ASME Pumping Machinery Symposium*, vol. 154, pp. 369–375, American Society Of Magazine Editors, New York, NY, USA, 1998.

[7] S. M. Miner, "3D viscous flow analysis of an axial flow pump impeller," in *Proc. 6th International Symposium on Transport Phenomena and Dynamics of Rotating Machinery (ISROMAC' 96)*, vol. 2, pp. 336–344, Honolulu, Hawaii, USA, February 1996.

[8] S. M. Miner, "3D viscous flow analysis of a mixed flow pump impeller," in *Proc. 7th International Symposium on Transport Phenomena and Dynamics of Rotating Machinery (ISROMAC' 98)*, vol. C, pp. 1492–1501, Honolulu, Hawaii, USA, February 1998.

[9] S. V. Patankar, *Numerical Heat Transfer and Fluid Flow*, Hemisphere Publishing, New York, NY, USA, 1980.